NASA Technical Memorandum 103982

208994
26 P

Correlation of Airloads on a Two-Bladed Helicopter Rotor

Francisco J. Hernandez and Wayne Johnson
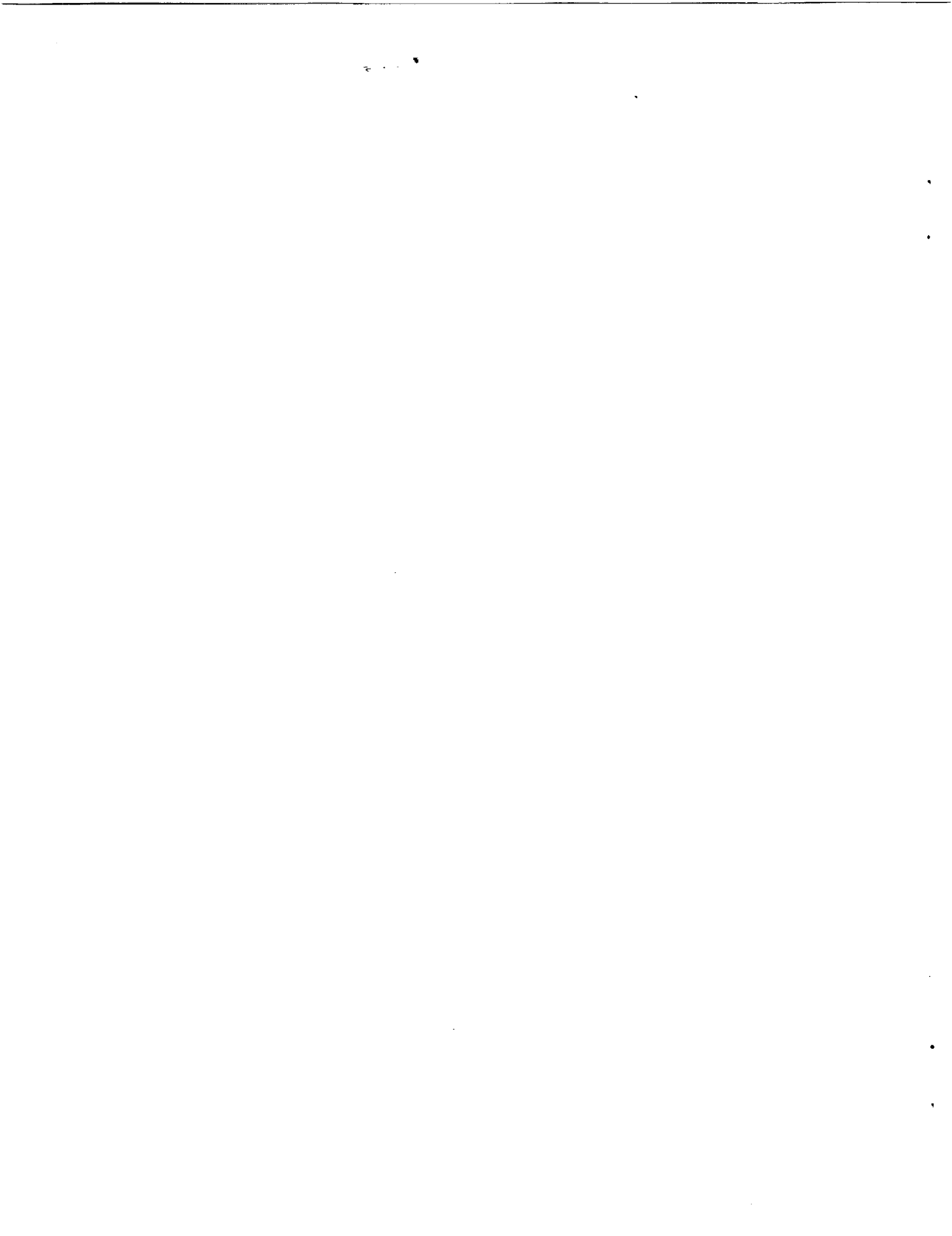
(NASA-TM-103982) CORRELATION OF
AIRLOADS ON A TWO-BLADED HELICOPTER
ROTOR (NASA) 26 p

N94-26143

Unclas

G3/02 0208994

April 1993

NASA
National Aeronautics and
Space Administration

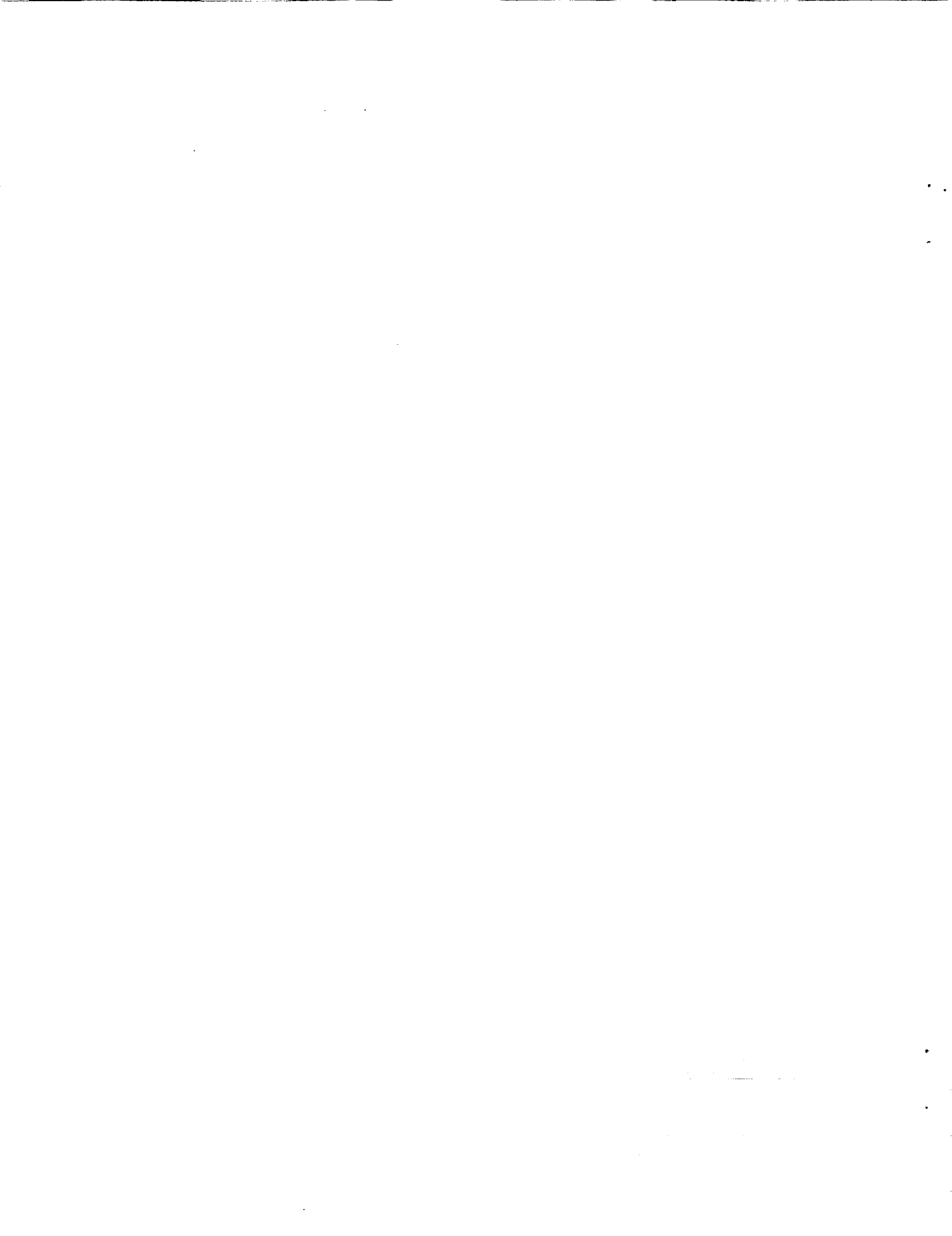# Correlation of Airloads on a Two-Bladed Helicopter Rotor

Francisco J. Hernandez, Ames Research Center, Moffett Field, California
Wayne Johnson, Johnson Aeronautics, Palo Alto, California

April 1993

NASA

National Aeronautics and
Space Administration

Ames Research Center
Moffett Field, California 94035-1000

Correlation of Airloads on a Two-Bladed Helicopter Rotor

FRANCISCO J. HERNANDEZ AND WAYNE JOHNSON*

Ames Research Center

Summary

Airloads measured on a two-bladed helicopter rotor in flight during the Ames' Tip Aerodynamic and Acoustic Test are compared with calculations from a comprehensive helicopter analysis (CAMRAD/JA), and the pressures compared with calculations from a full-potential rotor code (FPR). The flight-test results cover an advance ratio range of 0.19 to 0.38. The lowest-speed case is characterized by the presence of significant blade-vortex interactions. Good correlation of peak-to-peak vortex-induced loads and the corresponding pressures is obtained. Results of the correlation for this two-bladed rotor are substantially similar to those for three- and four-bladed rotors, including the tip-vortex core size for best correlation, calculation of the peak-to-peak loads on the retreating side, and calculation of vortex-induced loads on inboard radial stations. The higher-speed cases are characterized by the presence of transonic flow on the outboard sections of the blade. Comparison of calculated and measured airloads on the advancing side is not considered appropriate because the presence of shocks makes chordwise integration of the measured data difficult. However, good correlation of the corresponding pressures is obtained.

Nomenclature

c	blade chord
C_L	blade-section lift coefficient, $L/\frac{1}{2}\rho U^2 c$
C_N	blade-section normal force coefficient, $N/\frac{1}{2}\rho U^2 c$
C_p	blade-surface pressure coefficient, $p/\frac{1}{2}\rho U^2$
C_Q	rotor torque coefficient, $Q/\rho\pi R^2(\Omega R)^2 R$
c_s	speed of sound
C_T	rotor thrust coefficient, $T/\rho\pi R^2(\Omega R)^2$
$d(C_T/\sigma)/dr$	dimensionless blade-section lift, $L/\rho(\Omega R)^2 c$
L	blade-section lift (force per unit span)
M_{tip}	rotor-tip Mach number, $\Omega R/c_s$
M	blade-section Mach number, U/c_s
N	normal force (per unit span); number of blades
Q	main rotor torque
p	pressure
r	blade radial station, measured from center of rotation
R	rotor radius
T	rotor thrust
U	blade-section velocity (normal to span)
V	helicopter flight speed
x	chordwise distance from leading edge
α	angle of attack
α_{tpp}	rotor tip-path-plane angle, positive forward
β_c	rotor longitudinal tip-path-plane tilt relative to shaft, positive forward
β_s	rotor lateral tip-path-plane tilt relative to shaft, positive towards retreating side
μ	advance ratio, $V/\Omega R$
ρ	air density
σ, S	rotor solidity, $Nc/\pi R$
ψ	rotor azimuth angle, measured from downstream in direction of rotor rotation
Ω	rotor rotational speed

*Johnson Aeronautics, Palo Alto, California.

Introduction

The accurate prediction of rotor airloads is one of the most challenging problems in the field of theoretical aerodynamics and one that is far from being solved. The difficulties encountered making such predictions are caused by the highly complex nature of the rotor flowfield, which in forward flight includes compressibility effects on the advancing side, dynamic stall on the retreating side, and blade-vortex interactions. All of these features of the aerodynamic loading must be adequately handled before an accurate calculation of rotor performance, structural loads, or noise can be expected. This paper examines several issues involved in rotor airloads calculations, in particular focusing on blade-vortex interaction at low speed and the influence of transonic flow at high speed.

In order to look in detail at the factors that affect the accurate representation of the rotor aerodynamics, the comprehensive helicopter code CAMRAD/JA (ref. 1) was used to model the AH-1G rotor system. The results are compared with measured flight-test data on an AH-1G taken during the Tip Aerodynamic and Acoustic Test (TAAT) conducted at Ames Research Center (ref. 2). This is the first major correlation effort undertaken using the AH-1G airloads database.

The CAMRAD/JA model was used to calculate the performance, dynamics, and aerodynamic behavior of the rotor. The principal objective of the paper is to compare the measured and calculated blade-section lift at high and low speed. It is useful also to examine the pressure correlation for a subset of the results. For this purpose, the Full Potential Rotor code (FPR) was used (ref. 3), coupled with CAMRAD/JA to account fully for blade motion and wake effects. The pressure calculations are also of direct interest for predictions of rotor noise. This paper investigates the detailed pressure loading associated with the blade-section lift correlation.

The calculations are compared with flight measurements at different advance ratios ranging from $\mu = 0.19$ to 0.38. The lowest-speed case is characterized by the presence of significant blade-vortex interactions. The higher-speed cases are characterized by the presence of transonic flow on the outboard sections of the blade. This paper describes the flight test, the analytical methods used, the modeling of the AH-1G rotor, the assumptions made, and the resulting correlation between theory and flight measurements.

Tip Aerodynamic and Acoustic Test (TAAT)

The aircraft used during the Tip Aerodynamic and Acoustic Test (TAAT) was the first production AH-1G Cobra built (fig. 1). The AH-1G had a two-bladed,

teetering rotor with a constant-chord, rectangular-planform blade. The rotor radius was 22 ft. This flight-test program was conducted at NASA Ames Research Center during the early 1980s, using a set of highly instrumented rotor blades to study rotor-tip aerodynamics and acoustics. To accommodate the additional instrumentation (ref. 4), the blades used a symmetrical airfoil with a modified OLS (Operational Loads Survey) section. With this airfoil, the blade chord was increased from the standard 27.0 in. to 28.625 in., and the thickness-to-chord ratio was increased from 0.09330 to 0.09677. The rotor solidity was 0.06910, and the twist was linear from root to tip with a magnitude of -10 degrees. The gross weight of the aircraft was approximately 8000 lb.

The set of instrumented blades was developed for the U. S. Army Operational Loads Survey (OLS) test. For the TAAT, transducers at three new radial stations were added near the tip of the blade. The complete set of pressure transducer locations is shown in figure 2. Reference 2 presents a comprehensive description of the measurements with an analysis of the key phenomena.

Flight data from the TAAT test are stored on digital tapes and are available through DATAMAP (ref. 5). A cycle average of two rotor revolutions was used for the correlation with theory in this paper. DATAMAP was also used to process the data, making use of its large number of analysis tools, which include the derivation of the section load coefficients. The airloads database consists of six forward-speed cases and one hover condition, as shown in table 1. For this paper, all forward-speed cases were used, with special emphasis on the low-speed case of 82 knots and the high-speed case of 159 knots.

Analytical Methods

CAMRAD/JA

The blade airloading was calculated using the comprehensive helicopter code CAMRAD/JA (ref. 1). The rotor aerodynamic problem is based on lifting-line theory, using steady, two-dimensional airfoil characteristics and a vortex wake. The rotor wake model is based on a vortex lattice approximation of the wake. A small, viscous-core radius is used for the tip vortices. A large core size is used for the inboard wake elements to produce an approximation for sheet elements. A model of the wake rollup is included.

The analysis separates the aerodynamic problem into inner (wing), and outer (wake) problems, which are solved independently and then combined through a

Table 1. AH-1G TAAT operating conditions

Variable	Test points (counters)						
	2152	2153	2154	2155	2156	2157	2370
RPM	307.2	315.0	314.7	315.2	315.5	315.9	321.0
OAT, °C	11.5	18.5	18.5	18.5	18.5	18.5	16.5
Stat. press., psia	13.65	13.60	13.45	13.30	13.24	13.18	14.75
Airspeed, KTAS	159	146	129	116	98	82	0
μ	0.377	0.341	0.303	0.268	0.230	0.189	0.000
Gross weight, lb	8066	8000	7941	7920	7890	7870	9115
$C_T \times 100$	0.474	0.460	0.462	0.464	0.464	0.464	0.485
MR torque, in-lb	224310	184126	152109	130789	105313	93472	—
Long. flap., deg	−1.13	−1.87	−2.20	−2.38	−2.29	−2.13	−5.05
Lateral flapping, deg	−1.11	−0.60	−0.51	−0.19	−0.01	0.15	−4.12
Fuselage α, deg	−3.9	−1.7	−0.5	1.4	3.4	4.0	—
Pitch attitude, deg	−4.56	−2.36	−2.51	0.37	−0.16	0.89	−4.21
Long. cyc. pitch, deg	11.8	10.2	8.9	7.9	6.5	5.5	1.9
Lat. cyc. pitch, deg	−3.6	−2.4	−2.4	−2.1	−1.8	−1.7	2.4
Collective pitch, deg	18.0	15.8	14.5	13.4	12.2	11.7	14.4

matching procedure. The outer problem consists of an incompressible vortex wake from a lifting line, with distorted geometry. The inner problem consists of unsteady, compressible, viscous flow about an infinite-aspect-ratio, yawed wing. The inner problem is split into two-dimensional, steady, compressible, viscous flow (airfoil tables) with empirical corrections for unsteady aerodynamics, dynamic stall, and yawed flow. A detailed description of the aerodynamic analysis is given in reference 1.

The rotor structural model is represented by a section analysis based on engineering beam theory. The equations of motion are obtained from equilibrium of the inertial, aerodynamic, and elastic forces on the portion of the blade outboard of a particular blade section. The interface between the aerodynamics and dynamics models is defined by the section aerodynamic forces and the section velocities.

The wake-geometry models in CAMRAD/JA include: uniform inflow (linear variation of inflow over the rotor disk), nonuniform inflow with a prescribed wake geometry, and nonuniform inflow with a free wake geometry. As suggested in reference 6, for $\mu < 0.25$ the free wake analysis is used because of the highly distorted wake that remains close to the rotor plane. For higher advance ratios, where the wake is convected downward faster, a prescribed wake analysis gives the same accuracy and is more computationally efficient. These options were used in the computations performed for this paper.

FPR Code

The Full-Potential Rotor code (FPR) (ref. 3) was used to calculate the blade surface pressures. It was iteratively coupled with CAMRAD/JA to account fully for blade motion and wake effects. This code, developed by the U. S. Army at Ames Research Center, solves the unsteady, three-dimensional, full potential equation in conservation form. The code employs a finite-difference scheme that is solved using the method of approximate factorization. It has been demonstrated (ref. 7) that the FPR-CAMRAD/JA analysis produces nearly the same section lift as CAMRAD/JA, and hence is an appropriate tool to investigate the detailed pressure loading associated with the blade-section lift correlation.

The grid system used consists of a spanwise series of parallel O-grids. For the computation of rotor flows, an approximate rotational coordinate velocity is assigned to each grid point. Boundary conditions consist of a transpiration velocity at the surface, and nonreflection at the outer boundary.

A typical grid size used for the calculations for the AH-1G Cobra consists of 80 points in the chordwise direction, 25 in the spanwise direction, and 25 in the normal direction. The finite-difference grid extends in the spanwise direction approximately 4 chords inward of the

spanwise direction approximately 4 chords inward of the tip and 1.2 chords outward from the tip. The extent of this computational fluid dynamics (CFD) region is dependent on the advance ratio utilized in the calculation. At high advance ratios, the stalled region on the retreating side of the disk limits the inboard extent of the CFD domain. The outer boundary of the grid is located 5 chords from the surface of the blade. Constant time steps of 0.25 deg of azimuth angle were used for the calculations. Computer time for a 360-deg computation was approximately 1600 CPU seconds on the NASA Ames Cray Y-MP. Additional information on the FPR code can be found in references 3 and 7.

Model Description

The rotor aerodynamic tables utilized in the CAMRAD/JA model of the AH-1G were based on the Bell Helicopter Textron, Inc. (BHT)-developed 540 airfoil tables given in reference 4. The BHT 540 airfoil tables were generated from a wind-tunnel test, with standard corrections applied to maximum lift and profile drag. Because data were not available at high angle of attack and high Mach number, NACA 0012 tables are used, with a smooth transition between the two.

The 540 airfoil tables were modified using wind-tunnel data for the OLS/TAAT airfoil from a test conducted at NASA Langley Research Center (ref. 8). The OLS/TAAT airfoil was tested over a Reynolds-number range from 3×10^6 to 7×10^6, angles of attack from approximately –4 deg to 12 deg, and Mach numbers from 0.34 to 0.88 in the Langley 6- by 28-in. Transonic Tunnel. The BHT 540 airfoil tables were corrected using the Langley wind-tunnel data. The two databases were very similar, except at high Mach numbers. Using the Langley data introduced corrections to the maximum lift coefficient, the lift curve slope, and drag and moment coefficients at the stall condition. At the high Mach numbers, the Langley data were used, with a smooth transition to the NACA 0012 values. In all cases, symmetry between positive and negative angle of attack was imposed, including cases where the data did not indicate such behavior. This new airfoil table was used as part of the AH-1G CAMRAD/JA model.

The baseline for the OLS blade structural properties was taken from reference 4. Such data include blade mass, geometric twist, center of gravity offset, tension center offset, flapwise and chordwise bending stiffness, moment of inertia, polar radius of gyration, and torsional stiffness. Each structural property was generated in a stepwise manner for 48 segments as a function of blade radius. Some of the blade's structural characteristics are given in figure 3. For the OLS blade, the elastic axis is assumed to coincide with the feathering axis. The quarter chord of the

blade shifts aft 0.281 in. relative to the feathering axis at r/R = 0.31. This is caused by the addition of the instrumentation sleeve to the blade.

The calculated blade collective- and cyclic-mode frequencies are given in tables 2 and 3. These were obtained from the flutter analysis in CAMRAD/JA with no aerodynamics included. The boundary condition was teetering motion. The first four flapwise modes are identified along with the first two lag and torsion modes.

For the calculations, the rotor was trimmed to the measured flight conditions, defined by helicopter weight, shaft angle of attack, and longitudinal and lateral tip-path-plane angles relative to the shaft. These quantities are given in table 4 (ref. 2).

Here, $\alpha_{\tau pp}$ is the sum of the shaft angle and the longitudinal flapping relative to the shaft. In figure 4 these quantities are plotted vs. advance ratio. Notice the drastic change in tip-path-plane angle for advance ratios greater than 0.27.

In figure 5, the rotor-shaft torque coefficient is shown as a function of advance ratio. The disagreement at high advance ratios may be caused by the presence of dynamic stall. However, the calculated power for advance ratios above 0.34 follows the trend of the tip-path-plane tilt (which was the specified trim state in the calculations), suggesting that measurement of the shaft angle may be in error. The correlation is sufficient for the present purposes, however, since the airloads calculations are not very sensitive to the difference in measured and calculated propulsive force implied by figure 5.

Table 2. Collective-mode frequencies (per/rev)

Modes	Flap	Lag	Torsion
1st	1.109	1.631	2.656
2nd	3.107	10.709	7.656
3rd	5.227	---	---
4th	8.831	---	---

Table 3. Cyclic-mode frequencies (per/rev)

Modes	Flap	Lag	Torsion
1st	1.000	1.433	2.869
2nd	2.506	10.329	8.376
3rd	4.515	---	---
4th	7.502	---	---

Table 4. Flight-test conditions

V, knots	μ	α_{Tpp}, deg	C_T/σ	β_s, deg	β_c, deg
82	0.189	1.24	0.0672	0.15	2.13
98	0.230	2.45	0.0671	−0.01	2.29
116	0.268	2.75	0.0672	−0.19	2.38
129	0.303	4.71	0.0669	−0.51	2.20
146	0.341	4.23	0.0666	−0.60	1.87
159	0.377	5.68	0.0686	−1.11	1.13

Blade Airloads

The rotor airloads will be presented in the form of section lift around the azimuth, as defined by the following equation:

$$d(C_T/S)/dr = L/\rho(\Omega R)^2 c \qquad (1)$$

The experimental data provided the normal force, which for small angle of attack ($C_L \cong C_N$) and a constant chord blade can also be written in the form:

$$d(C_T/S)/dr = \frac{1}{2M_{\text{tip}}^2} M^2 C_N \qquad (2)$$

Equation (2) was used to convert the flight data into the same form as the section lift given by the calculations in equation (1).

As a check on the AH-1G flight-test data, the total rotor lift was calculated and compared with the gross weight of the aircraft. This was accomplished by integrating the blade pressures chordwise and computing the azimuthal average of the section lift over the rotor disk. The thrust was then calculated by integrating the section lift over the blade radius. For the case of V = 82 knots, a rotor thrust of 7989 lb was obtained, which corresponds to an aircraft weight of 7870 lb. The difference between the thrust and gross weight might be caused by a download on the fuselage created by the rotor downwash. Again, the correlation is sufficient for the present purposes, since the airloads calculations are not particularly sensitive to a thrust change of this magnitude.

Discussion of Results: Low-Speed Cases

Effect of Torsional Degrees of Freedom

The AH-1G rotor blade has a fundamental pitch/torsion frequency below 3/rev (tables 2 and 3), so the possibility of a significant effect of the blade dynamics on the airloads was anticipated. To examine this effect in detail, a parametric study was done on the first and second blade torsional degrees of freedom. Figure 6 shows the effect of different combinations of torsional degrees of freedom on the blade loading at r/R = 0.91 and r/R = 0.97. It is seen that the effects occur on the front part of the rotor disk, where the blade undergoes the greatest torsional loads. Minor differences are seen between the different options, but using both first and second torsion degrees of freedom, the calculations correlate slightly better with the flight measurements. This option was selected as the baseline for all subsequent calculations.

Effect of Tip-Vortex Core Size

Because of its great effect in blade airloads, specifically on blade-vortex interaction, the size of the tip-vortex core was varied in the calculations to establish the most appropriate size for each flight condition. The tip-vortex core radius determines the maximum velocity induced by the vortex. Core sizes ranging from 0.015R to 0.040R (approximately 15 to 40% chord) were used and compared with flight data at different radial stations. Figure 7 shows such a comparison for V = 82 knots at several radial stations on the blade. The calculations overpredict the loading on the front part of the disk and underpredict the magnitude on the forth quadrant. This overprediction occurs for all radial stations examined.

Significant blade-vortex interaction is seen at the 90-deg-and 270-deg-azimuth stations. The core size has a modest influence on the peak-to-peak vortex-induced loading on the advancing side, but no influence on the retreating side. This indicates that there is a large vertical separation of the tip vortex from the blade; hence the loads are not sensitive to tip-vortex core radius. Rather, the loads are more dependent on the strength of the vortex than on its peak velocities. Peak-to-peak amplitudes are well matched on

the retreating side. Peak-to-peak amplitudes are under-predicted for r/R = 0.864 on the advancing side. For the outboard stations, smaller core sizes generally give a better representation of the peak-to-peak amplitudes (fig. 7(e) is an expanded view for r/R = 0.91).

This two-bladed rotor exhibits less of an influence of core size on the airloads than would be seen for a three- or four-bladed rotor at the same advance ratio, since with two blades, the tip vortex has more time to convect between its creation and its interaction with the following blade. While it is therefore more difficult to deduce the core size based on the present data, it appears that a core radius of about 20% chord is a good choice. This is approximately the same core radius found to be appropriate for three- and four-bladed rotors in reference 9. Notice also that the vortex-induced loads tend to be overpredicted on the retreating side (a feature also observed in reference 9 for three- and four-bladed rotors). Since for this case the retreating-side blade-vortex interaction is not sensitive to core size, this discrepancy may be caused by partial tip-vortex rollup. The tip vortex may not be completely rolled up by the time it reaches the following blade, so the strength may be less than the value of peak bound circulation (as assumed in the calculation).

In figure 8, the influence of core size is shown for V = 98 knots at r/R = 0.91, r/R = 0.955, and r/R = 0.97. The results are similar to those of the previous case, the calculations exhibiting only modest influence of core size on the advancing side and none on the retreating side. In order to explore this lack of sensitivity to core size in these two cases, a lower-speed case of V = 43 knots (for which no flight-test data were available) was examined. Figure 9 shows this case, in which a more significant effect of core size is seen in both the advancing and retreating side of the disk. This confirms the assumption that, at 82 knots, the blade vortex passes the blade at a large vertical distance; thus the core size has a negligible effect.

In all cases analyzed, small core sizes of about 0.020R showed a slightly better correlation and were used as baseline for the following calculations.

Inboard Blade-Vortex Interaction

Figure 10 shows the airloads calculated using an inboard core size of 0.02R, on both outboard and inboard radial stations. Although good calculation of peak-to-peak vortex-induced loads is achieved on outboard stations (r/R > 0.91), the oscillatory loads are significantly overpredicted on inboard stations when this core size is used. CAMRAD/JA can simulate this effect (with no implication that the physics of the phenomenon are understood,

however) by using a larger core size when calculating the vortex-induced velocities at inboard collocation points on the blade. Figure 10 also shows the improved correlation produced by this model, using a core size of 0.14R for inboard stations (transitioning to 0.02R for radial stations from r/R = 0.76 to 0.88). It is therefore observed that when the vortex-induced loads are calculated using a core size that gives good correlation at the blade tip, the strength of the blade-vortex interactions is significantly overpredicted for inboard stations. This phenomenon has been observed in other correlation studies as well (ref. 9).

Blade-Surface Pressure Distributions

Calculated blade-surface pressure distributions for V = 82 knots are given in figure 11 at r/R = 0.910 for azimuths on the advancing and retreating side (near the blade-vortex interactions). Data for the last chordwise pressure transducer (x/c = 0.91) were not available for this radial station. On the advancing side, calculations underpredict the blade upper-surface pressures, especially the pressure rise close to the leading edge. Better correlation is seen on the retreating side, except at 300 deg azimuth. This correlation is consistent with the airloads results (fig. 7(b)), where better correlation was obtained for the retreating-side blade-vortex interaction.

Figure 12 shows similar pressure correlations for r/R = 0.97 (corresponding to airloads in fig. 7(d)). Again, the calculations underpredict the blade-surface pressures throughout the rotor disk. At inboard radial stations the surface pressure correlation was better, as evidenced in figure 13 for r/R = 0.60 at three azimuths on the advancing side (corresponding to airloads in fig. 10(b)).

Low-Speed Airloads Correlation

The present paper and reference 9 compare the measured and calculated airloads for the three cases given in table 5. All the rotors considered had rectangular planforms (except for the trapezoidal tip cap of the H-34) and linear twist (except for zero twist at the tip of the SA349/2). These three cases exhibit the following common behavior:

a) Good correlation with measured peak-to-peak vortex-induced loads is obtained using a tip-vortex core radius of

Table 5. Low-speed airloads correlation cases

Rotor	N	σ	c/R	C_T/σ	μ
AH-1G	2	0.069	0.101	0.067	0.19
SA349/2	3	0.064	0.067	0.065	0.14
H-34	4	0.062	0.049	0.082	0.18

approximately 20% chord. This value is in the range of measured core sizes for rotor wakes, although it is probably still somewhat too large.

b) With a single tip-vortex core size for the wake model, and assuming that the strength of the tip vortex equals the peak bound circulation of the blade when the vortex is generated, there is a tendency to overpredict the peak-to-peak loads on the retreating side and underpredict on the advancing side. This result suggests that, on the retreating side, the core size is larger, or that the vortex strength is less than the peak bound circulation.

c) Something is happening on the inboard part of the blade to reduce the measured vortex-induced loads. References 6 and 9 speculate that this effect is associated with a smaller blade-vortex separation calculated for interactions on the inboard part of the blade than that calculated for interactions at the tip of the blade.

Discussion of Results: High-Speed Cases

Blade Airloads

Airloads were calculated for the higher-speed cases present in the database, using the baseline parameter values determined for 82 knots. Figure 14 compares the measured and calculated airloads at 159 knots ($\mu = 0.377$). For all the tip radial stations shown, the measured section lift exhibits a roughly constant value in the first quadrant of the disk before dropping to near or below zero at about 90 deg azimuth. In contrast, the aerodynamic mechanisms present in the calculation produce a continuous decrease of the section lift in the first quadrant, as would be expected because of roll moment balance. There is a slight bump in the calculated airloads, produced by interaction with the tip vortex from the preceding blade. In the analysis (ref. 6), the tip vortex has negative strength in this region, since the tip loading is negative. Figure 15 compares measured and calculated airloads for speeds of 116, 129, and 146 knots. The results are similar to those at 159 knots. The behavior of the measured airloads, and the resulting correlation with calculations, have been observed in investigations of high-speed airloads with other rotors (ref. 6). For this two-bladed rotor, with constant airfoil and low-aspect-ratio blades, significant compressibility effects occur even at relatively low advance ratios (fig. 15).

The nearly constant lift present in the plotted experimental data on the advancing side may be caused by difficulties in determining the proper shock location during data reduction. As an example, figure 16 shows the measured pressure coefficient at 75 deg azimuth, where the shock

appears between the x/c = 0.25 and 0.35 pressure transducers. The baseline section lift is obtained using direct interpolation between the measured pressures (fig. 16(a)). Figures 16(b) and 16(c) show alternate interpretations of the pressure change associated with the shock, which will produce integrated lift coefficients higher and lower than the baseline. Figure 17 shows the measured and calculated section lift and lift coefficient, including, for several azimuths, results of these alternate interpretations of the flight-test data. The correlation between calculated and measured airloads is evidently very sensitive to such interpretations. Notice also that considering lift rather than lift coefficient magnifies the differences, because it is the advancing side that is of interest.

Another phenomenon present in the experimental data at this flight condition is the sharp bump in section lift at r/R = 0.955, seen in the second quadrant (e.g., fig. 14(c)). A similar effect has been observed in flight and wind-tunnel data on other rotors. To examine this effect, figure 18 presents the surface pressures before, at, and after the peak lift. The pressures indicate that at 120 deg azimuth there is a strong shock wave present on both upper and lower surfaces that rapidly decreases in magnitude at 135 deg and is non-existent at 150 deg azimuth. Because of the absence of pressure tranducers on the lower surface between 5% and 25% chord, direct interpolation of the pressures (as illustrated by fig. 18(b)) produces a sharp rise in the integrated section lift as soon as the lower-surface shock moves forward of 25% chord. Hence this and other sharp changes in the measured section lift are most likely attributable to a lack of sufficient data to define the movement of the shocks on the advancing side of the blade, rather than to any aerodynamic phenomenon of rotor blades in transonic flow.

Given the difficulties associated with making a highly instrumented rotor blade, it may be impossible to achieve a chordwise and spanwise resolution sufficient to examine all aerodynamic phenomena. A more sophisticated method of integrating the pressures to obtain section lift, specifically one that estimates the shock location implied by the data, would be most useful for future tests. For the present investigation, it is concluded that there is little to be gained by trying to compare the measured and calculated section lift.

Blade-Surface Pressure Distributions

Figures 19 and 20 compare the measured and calculated blade-surface pressure coefficients for V = 159 knots at r/R = 0.970, for several azimuths in the first and second quadrants, respectively. Transonic flow is seen to be present at 30 deg azimuth and becomes more dominant close to 90 deg. The shock strength and location are well

predicted by the calculations. Upper-surface pressures are underpredicted in most cases. The phenomena evident in the measurements are generally captured by the calculations, with the exception of the delay in formation of the lower-surface shock at 60 deg azimuth.

Conclusions

Airloads calculations were performed for a two-bladed rotor using a comprehensive helicopter analysis and were correlated with flight-test data. Fairly good correlation of peak-to-peak vortex-induced loads was obtained for a low-speed case. Sensitivity to tip-vortex core size at this speed was observable but small on the advancing side, and negligible on the retreating side. This relative insensitivity to core size (compared to a four-bladed rotor at the same advance ratio) is attributed to a larger vertical separation of the tip vortex from the blade. Therefore, the peak-to-peak loading is more dependent on the vortex strength than on the core size. Nonetheless, the results of the correlation for this two-blade rotor were substantially similar to the results for three- and four-bladed rotors, concerning the tip-vortex core size for best correlation, calculation of the peak-to-peak loads on the retreating side, and calculation of vortex-induced loads on inboard radial stations.

Blade-surface pressures for the low-speed case correlated reasonably well with flight data, particularly on the retreating side. This was consistent with the section lift correlation, where the second blade-vortex interaction was better matched.

Airloads were calculated for the higher-speed cases present in the database. All cases showed similar differences between the calculations and the flight measurements. In particular, the measured section lift exhibited a roughly constant value in the first quadrant before dropping to near zero, whereas the calculations show a continuous decrease of the section lift. It was speculated that the behavior of the flight data was caused in part by difficulties determining the shock location when integrating the measured pressures. It was demonstrated that sharp changes in the measured section lift are most likely attributable to a lack of sufficient pressure transducers to define the movement of the shocks on the advancing side of the blade. For the present investigation, it was concluded that there is little to be gained by trying to compare the measured and calculated section lift.

Blade-surface pressures were compared for the high-speed case and correlated fairly well with flight data, even where measured and calculated lift disagreed. Shock location and magnitude were good, but upper-surface pressures were underpredicted in most cases. The phenomena evident in the measurements were generally captured by the calculations, with the exception of the delay in formation of the lower-surface shock in the first quadrant.

References

1. Johnson, W.: A Comprehensive Analytical Model of Rotorcraft Aerodynamics and Dynamics, Johnson Aeronautics Version. Johnson Aeronautics, 1988.

2. Cross, J. L.; and Watts, M. E.: Tip Aerodynamic and Acoustic Test. NASA RP-1179, December 1988.

3. Strawn, R. C.; and Caradonna, F. X.: Conservative Full-Potential Model for Unsteady Transonic Rotor Flows. AIAA J., vol. 25, no. 2, February 1987.

4. Van Gaasbeek, J. R.: Validation of the Rotorcraft Flight Simulation Program (C81) using Operational Loads Survey Flight Test Data. USAAVRADCOM-TR-80-D-4, July 1980.

5. Philbrick, R. B.: The Data from Aeromechanics Test and Analytics—Management and Analysis Package (DATAMAP), Volume 2—Systems Manual. USAAVRADCOM-TR-80-D-30B, December 1980.

6. Johnson, W.: Wake Model for Helicopter Rotors in High Speed Flight. NASA CR-177507, November 1988.

7. Strawn, R.C.; Dessoper, A.; Miller, J.; and Jones, A.: Correlation of Puma Airloads—Evaluation of CFD Prediction Methods. NASA TM-102226, August 1989.

8. Watts, M. E.; Cross, J. L.; and Noonan, K. W.: Two-Dimensional Aerodynamic Characteristics of the OLS/TAAT Airfoil. NASA TM-89435, April 1988.

9. Johnson,W. Calculation of Blade-Vortex Interaction Airloads on Helicopter Rotors. J. Aircraft, vol. 26, no. 5, May 1989.

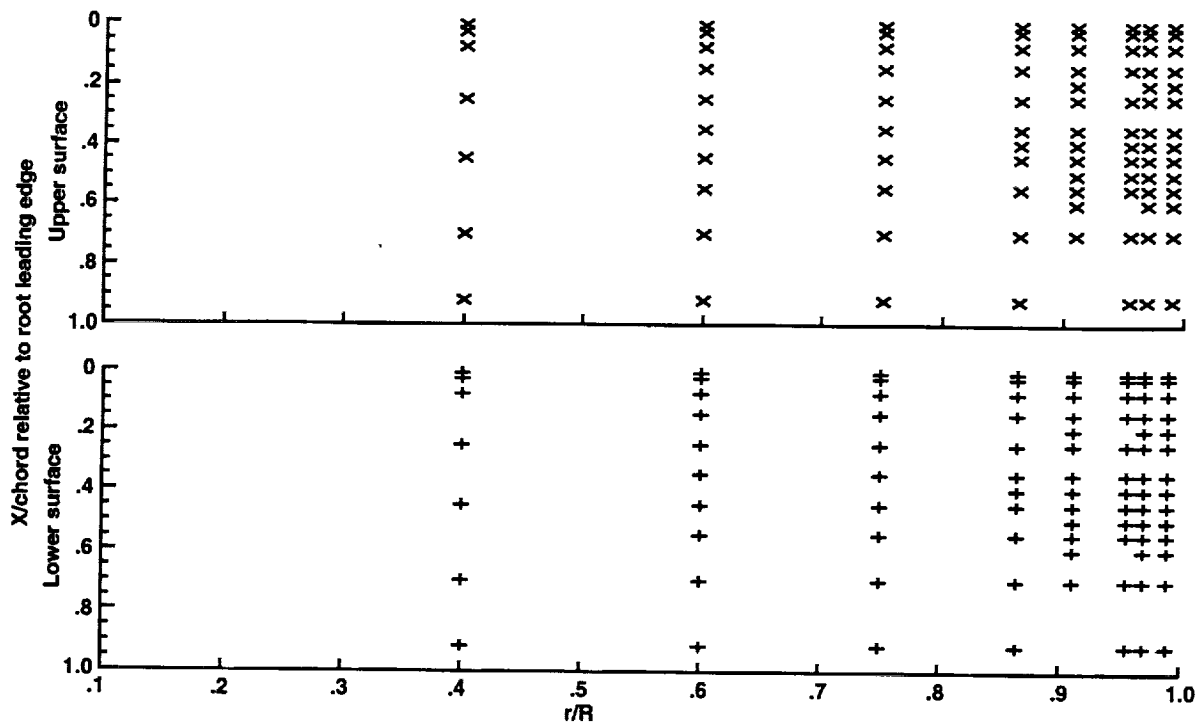Figure 1. AH-1G Cobra test helicopter at NASA Ames.

Figure 2. AH-1G TAAT blade pressure instrumentation locations (94 upper, 94 lower transducers).
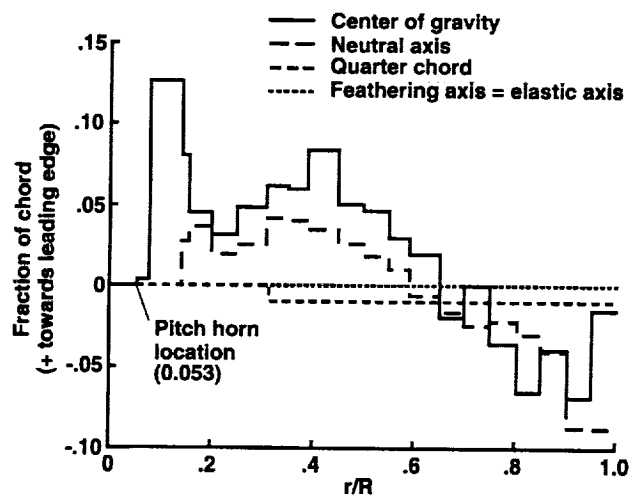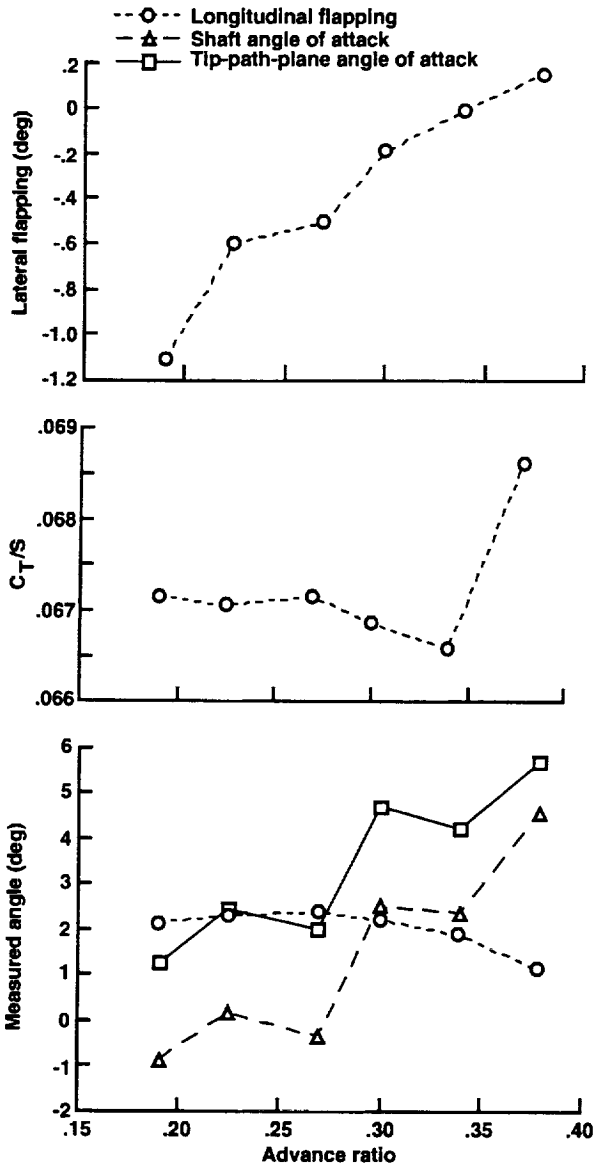

Figure 3. AH-1G blade description.

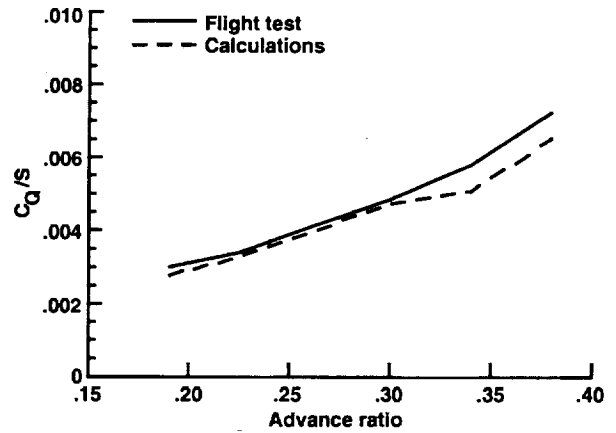Figure 4. *Trim quantities used in the analysis.*

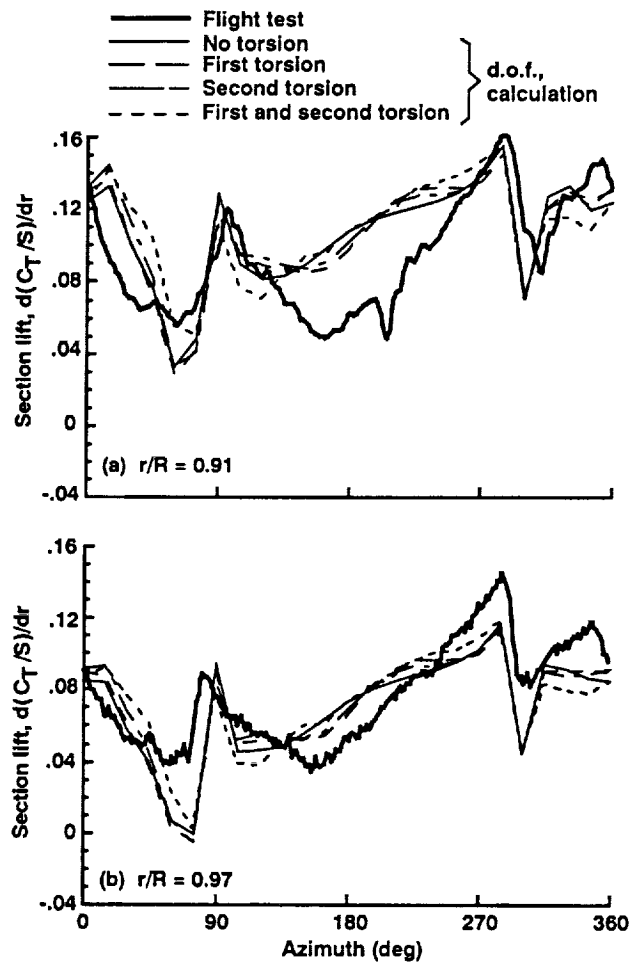Figure 5. *Rotor shaft torque coefficient vs. advance ratio.*

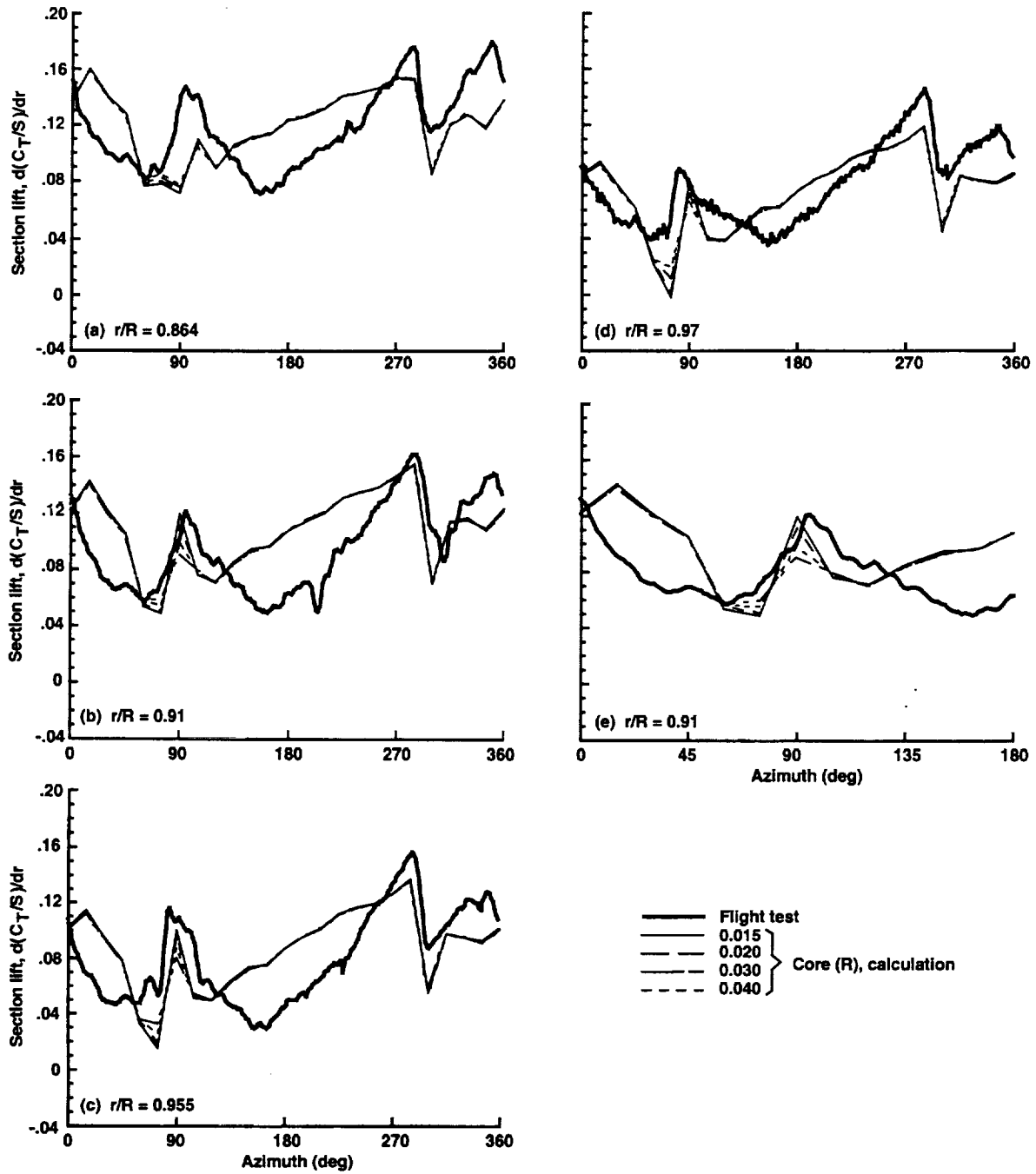Figure 6. Influence of torsion degrees of freedom on airloads (V = 82 knots).

12

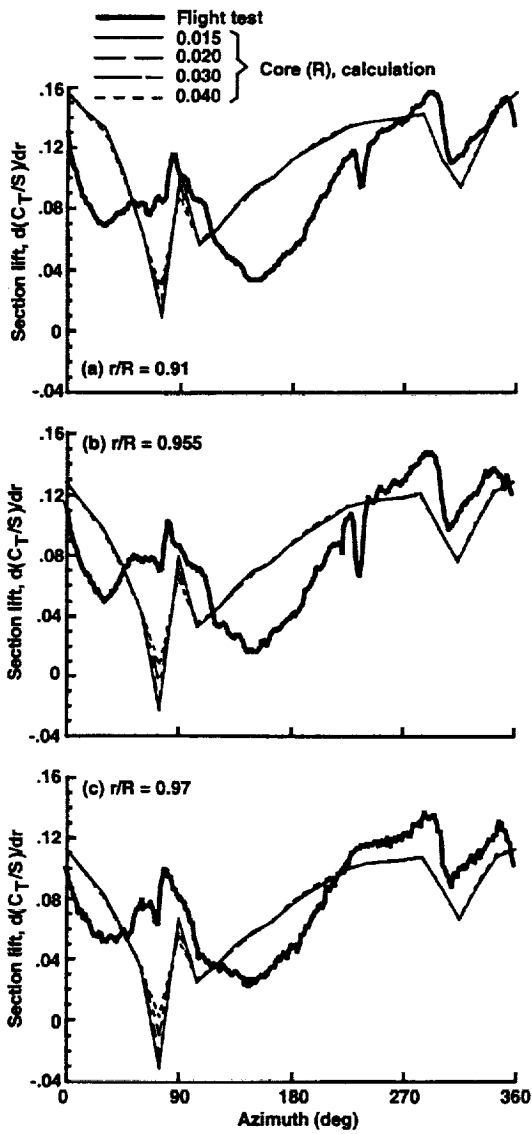Figure 7. Effect of vortex core size on airloads (V = 82 knots).

13

Figure 8. Effect of vortex core size on airloads
(V = 98 knots).
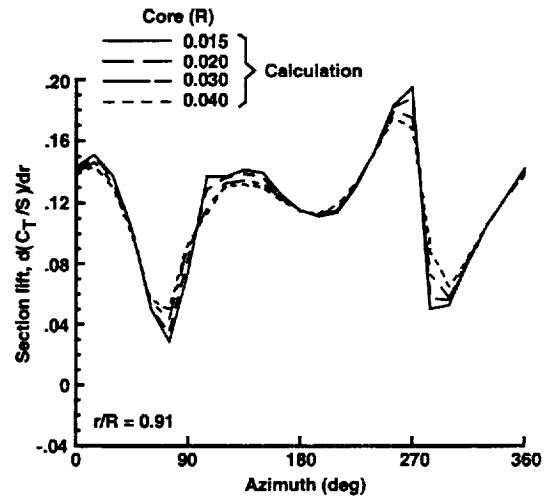
Figure 9. Effect of vortex core size on airloads
(V = 43 knots, μ = 0.10).
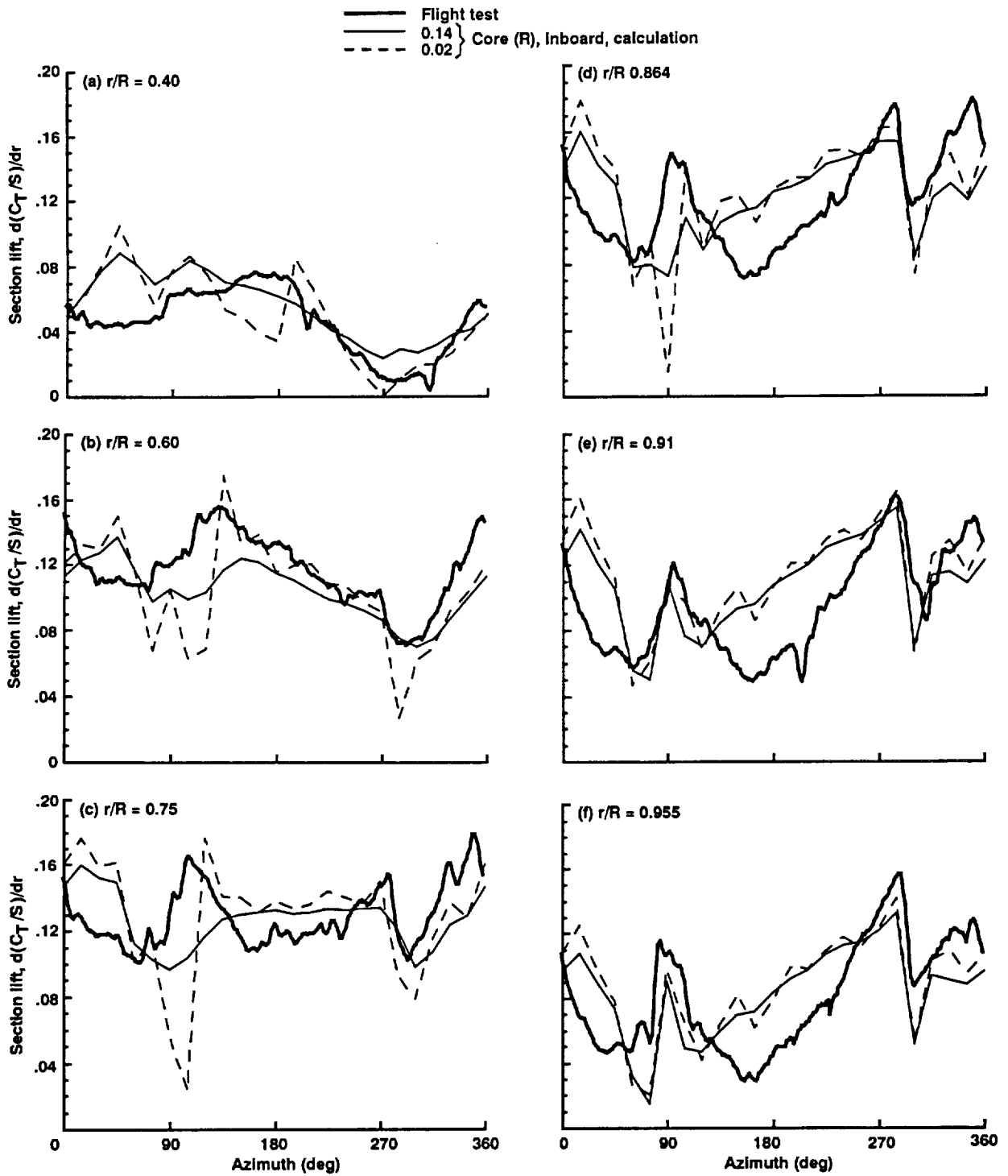
Figure 10. Effect of inboard core size on airloads (V = 82 knots).
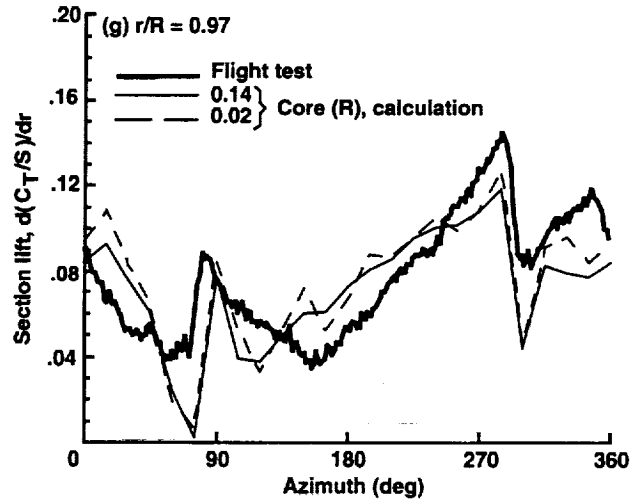
Figure 10. Concluded.
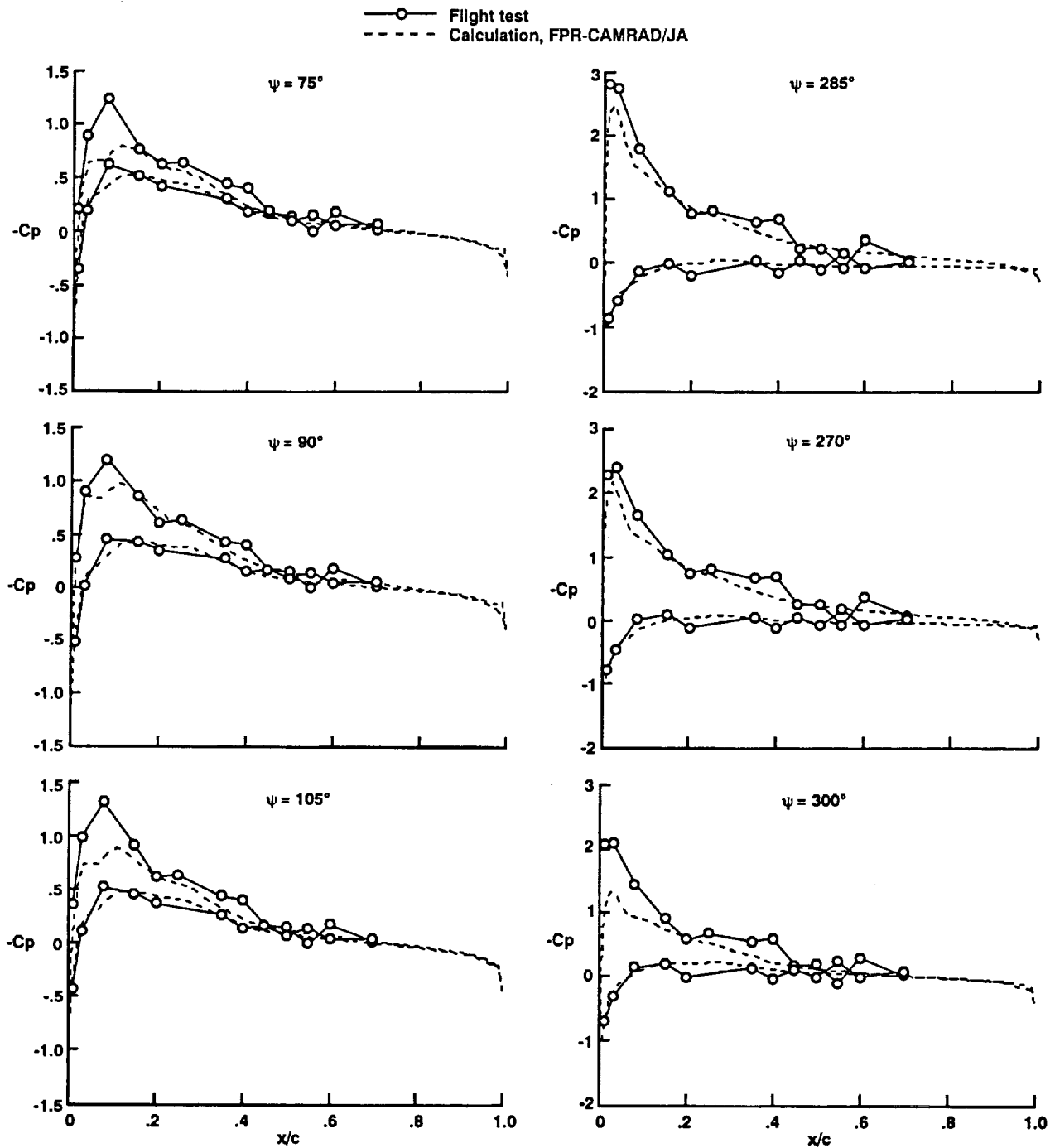
Figure 11. Calculated and measured blade-surface pressure distributions (V = 82 knots, r/R = 0.910).
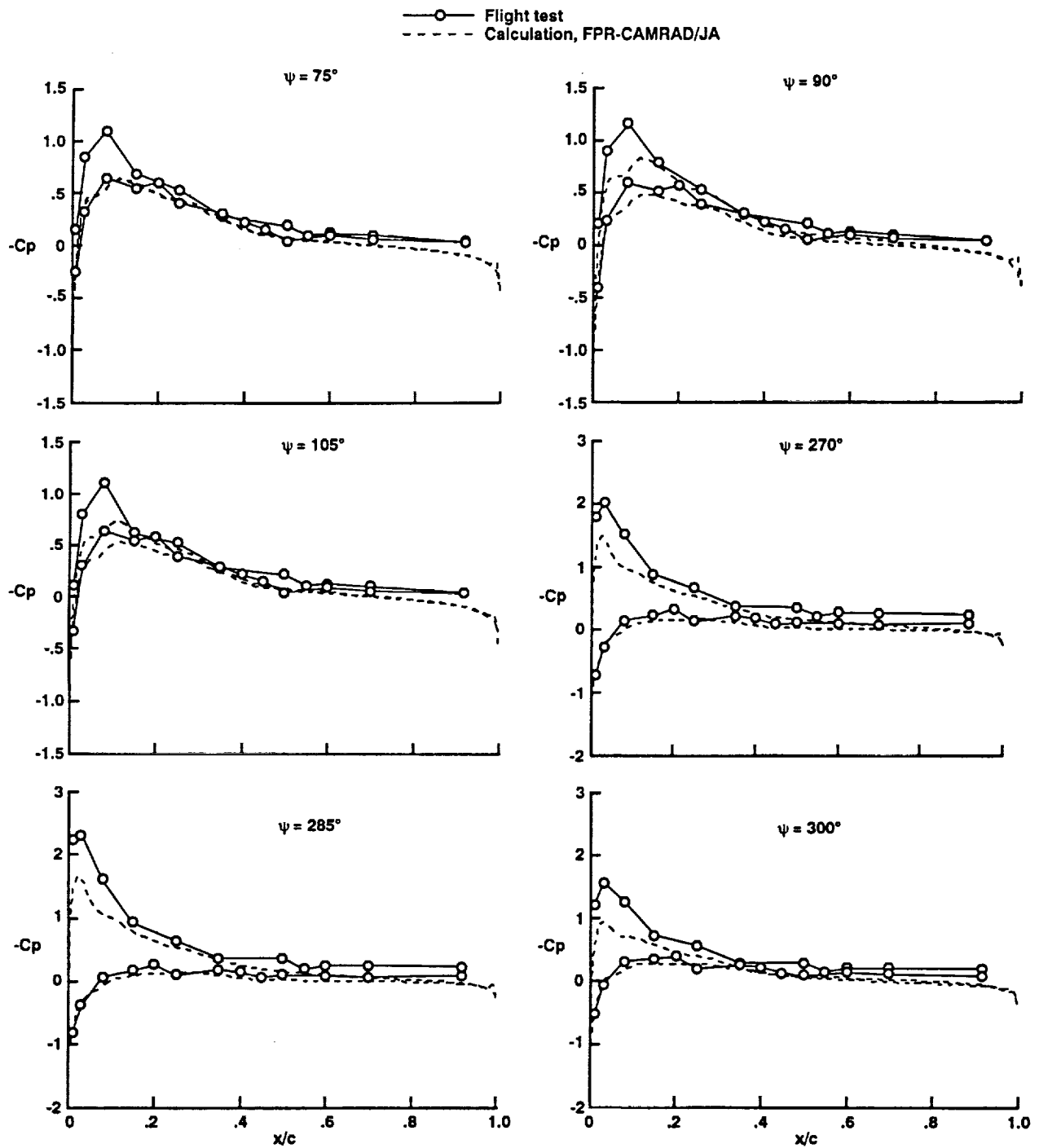
Figure 12. Calculated and measured blade-surface pressure distributions (V = 82 knots, r/R = 0.970).
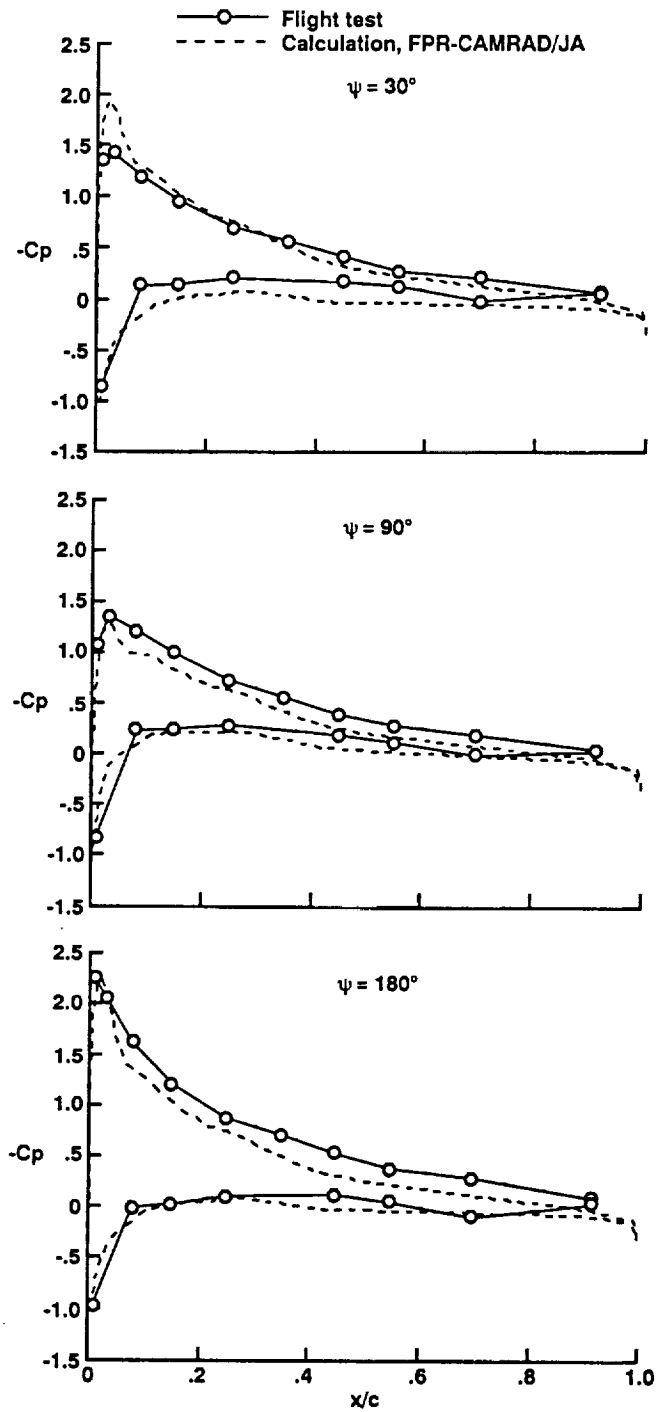
Figure 13. Calculated and measured blade-surface pressure distributions (V = 82 knots, r/R = 0.60).
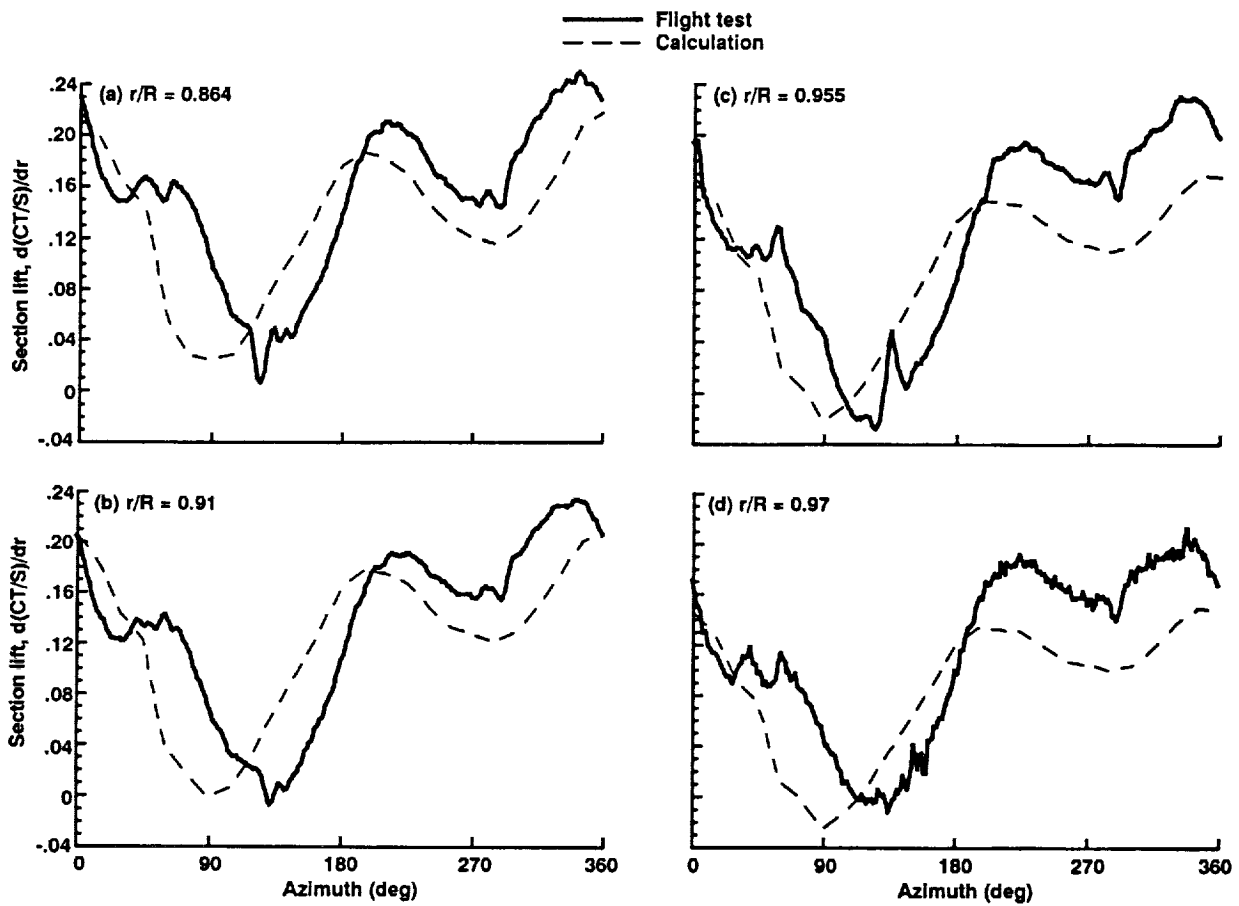
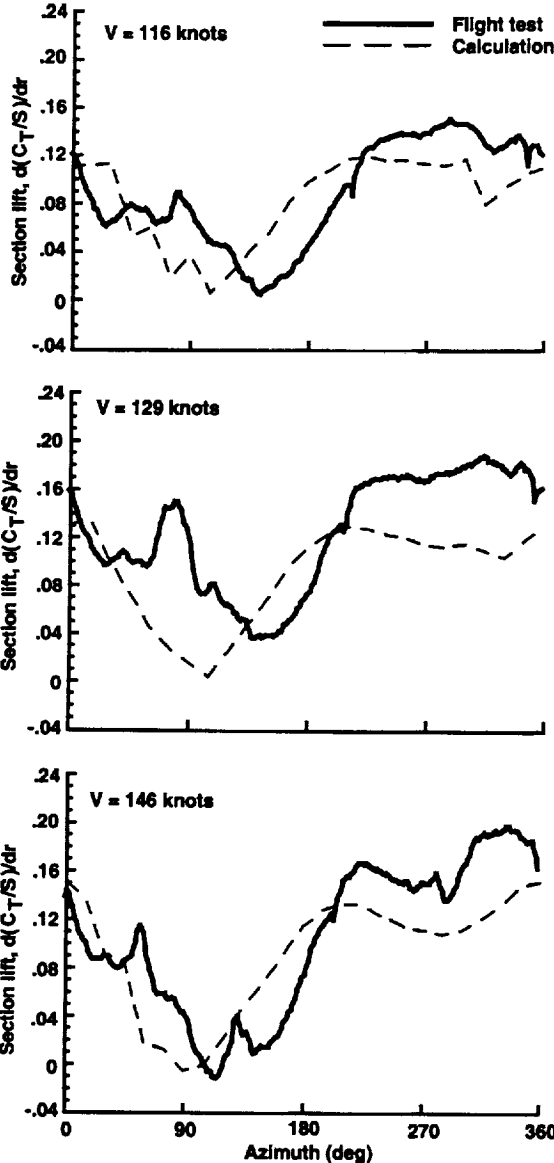Figure 14. Calculated and measured blade-section lift (V = 159 knots).

20

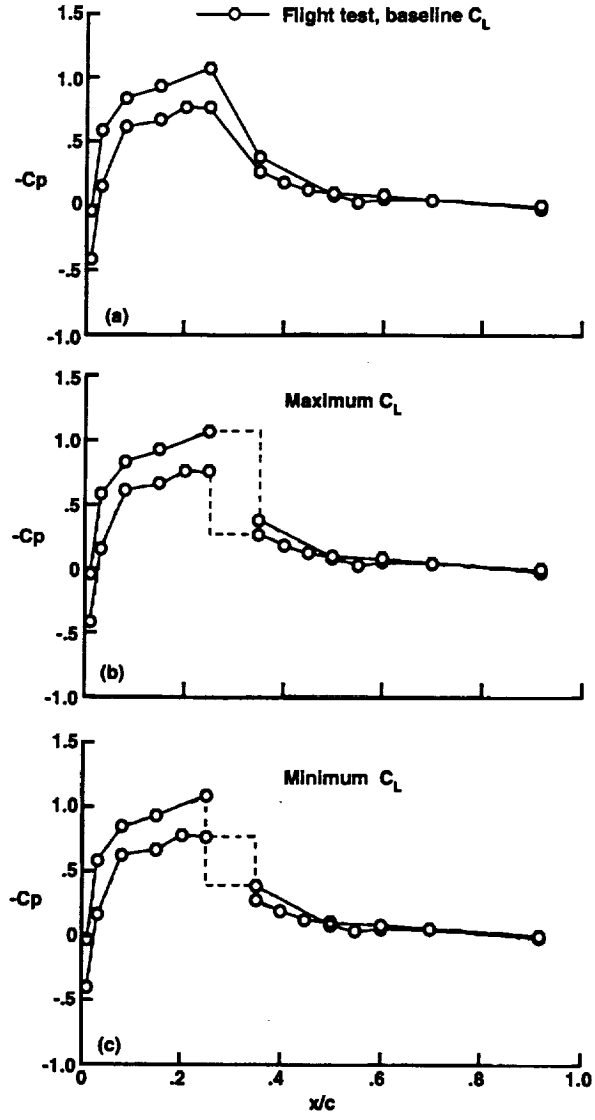Figure 15. Calculated and measured blade-section lift at different advance ratios (r/R = 0.955).

Figure 16. Determination of maximum and minimum lift due to shock location (V = 159 knots, r/R = 0.970, y = 75°).
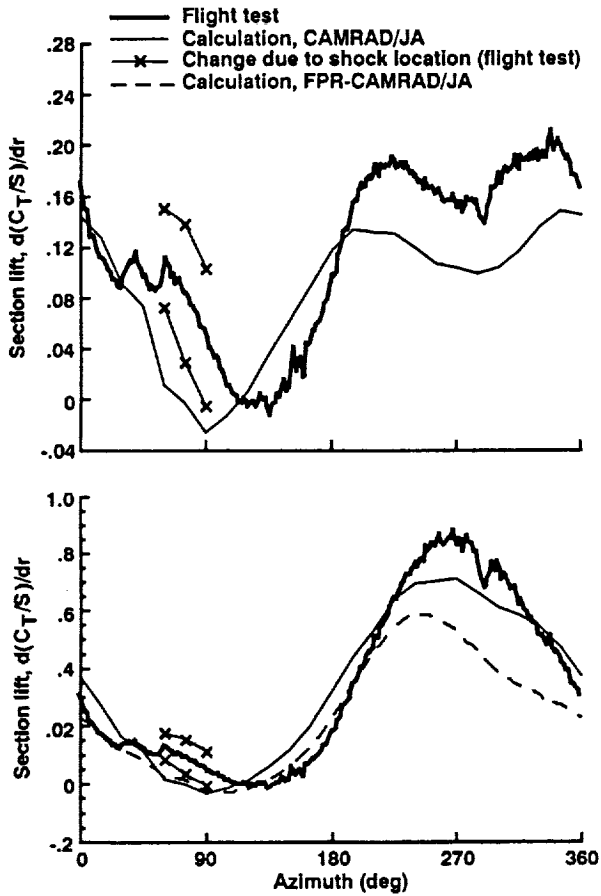
Figure 17. Maximum change in section lift and lift coefficient to shock location (V = 159 knots, r/R = 0.970).
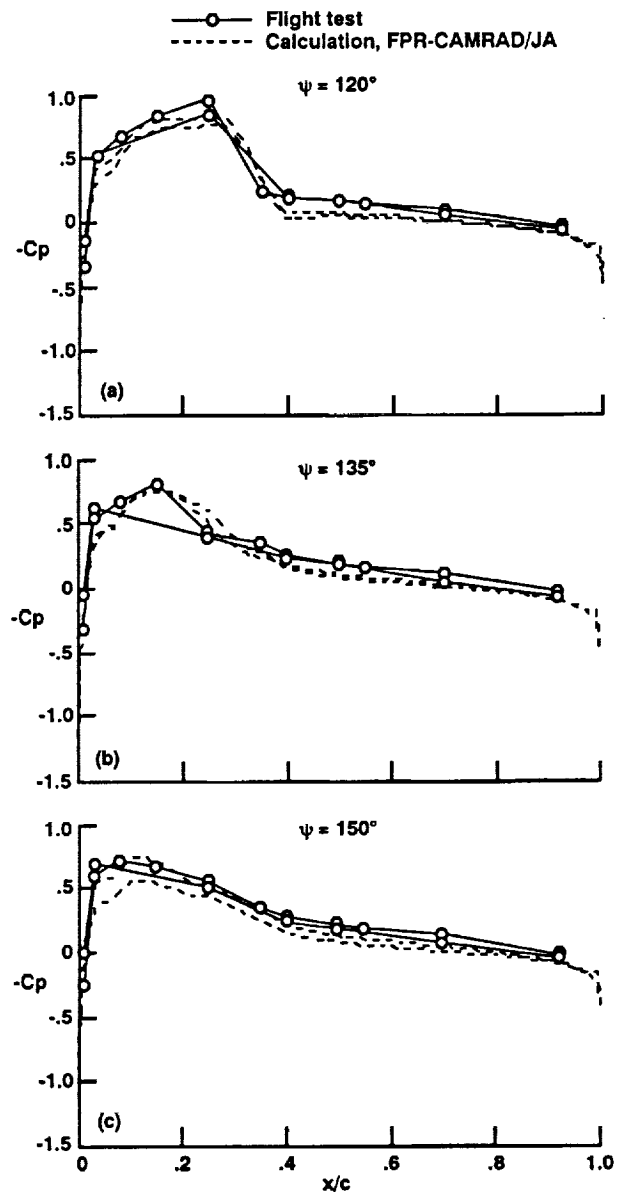

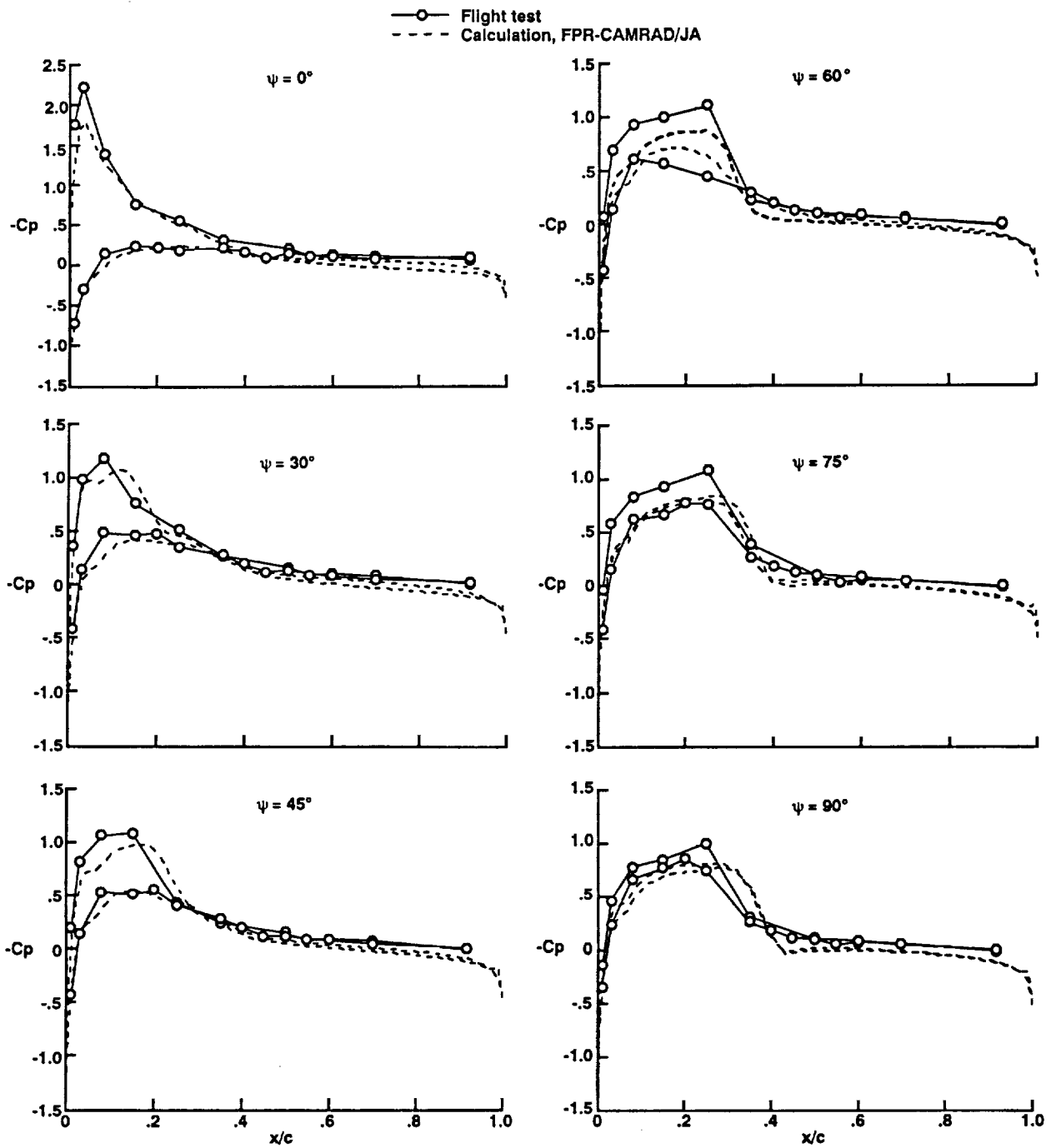Figure 18. Blade-surface pressures at section lift bump (V = 159 knots, r/R = 0.955).

22

Figure 19. Calculated and measured blade-surface pressure distributions (V = 159 knots, r/R = 0.970).

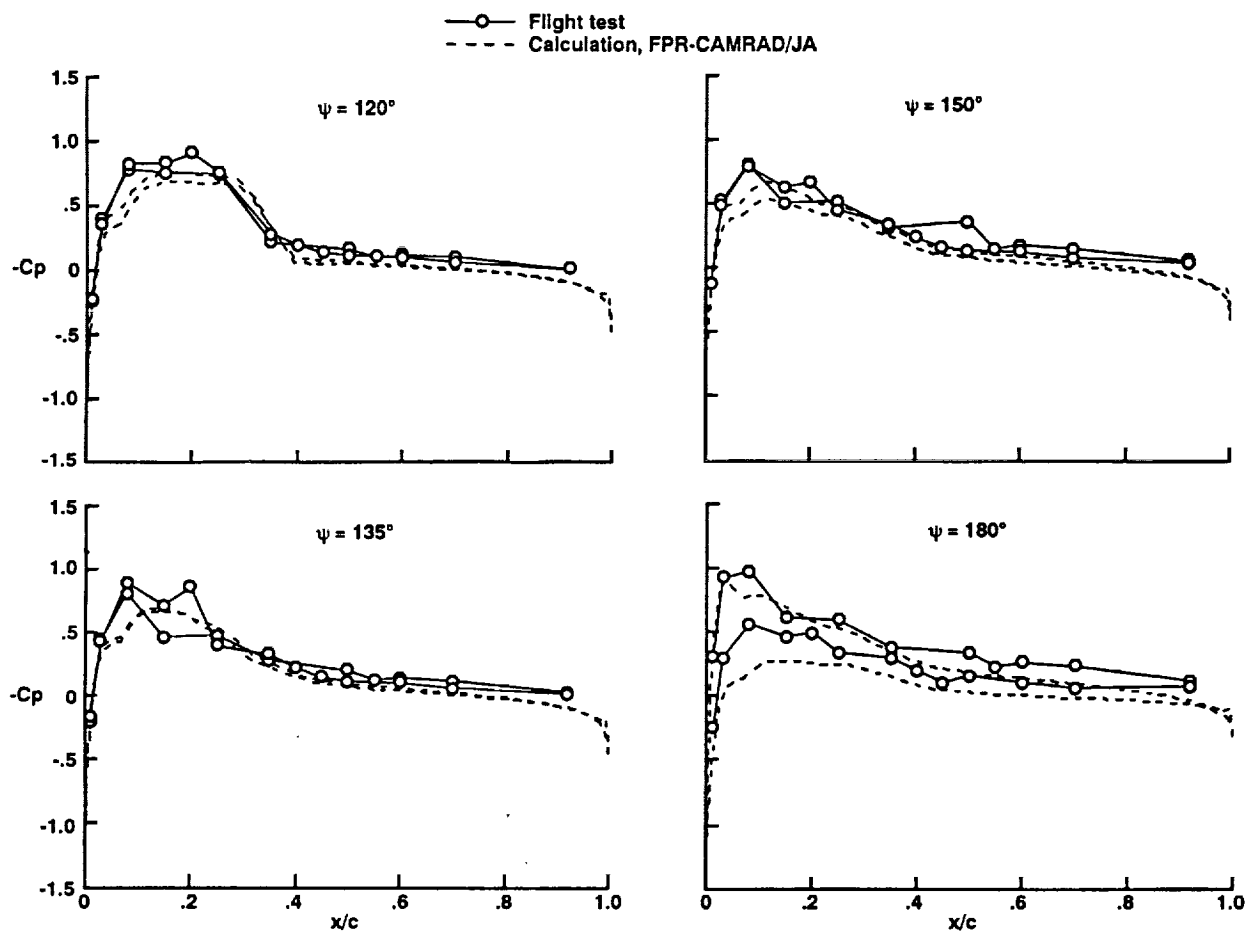Figure 20. Calculated and measured blade-surface pressure distributions (V = 159 knots, r/R = 0.970).

REPORT DOCUMENTATION PAGE

Public reporting burden for this collection of information is estimated to average 1 hour per response, including the time for reviewing instructions, searching existing data sources, gathering and maintaining the data needed, and completing and reviewing the collection of information. Send comments regarding this burden estimate or any other aspect of this collection of information, including suggestions for reducing this burden, to Washington Headquarters Services, Directorate for information Operations and Reports, 1215 Jefferson Davis Highway, Suite 1204, Arlington, VA 22202-4302, and to the Office of Management and Budget, Paperwork Reduction Project (0704-0188), Washington, DC 20503.

1. AGENCY USE ONLY (Leave blank)	2. REPORT DATE April 1993	3. REPORT TYPE AND DATES COVERED Technical Memorandum

4. TITLE AND SUBTITLE	5. FUNDING NUMBERS
Correlation of Airloads on a Two-Bladed Helicopter Rotor **6. AUTHOR(S)** Francisco J. Hernandez and Wayne Johnson (Johnson Aeronautics, Palo Alto, California)	505-59-36

7. PERFORMING ORGANIZATION NAME(S) AND ADDRESS(ES)	8. PERFORMING ORGANIZATION REPORT NUMBER
Ames Research Center Moffett Field, CA 94035-1000	A-93001

9. SPONSORING/MONITORING AGENCY NAME(S) AND ADDRESS(ES)	10. SPONSORING/MONITORING AGENCY REPORT NUMBER
National Aeronautics and Space Administration Washington, DC 20546-0001	NASA TM-103982

11. SUPPLEMENTARY NOTES

Point of Contact: Francisco J. Hernandez, Ames Research Center, MS 237-5, Moffett Field, CA 94035-1000
(415) 604-1322

12a. DISTRIBUTION/AVAILABILITY STATEMENT	12b. DISTRIBUTION CODE
Unclassified-Unlimited Subject Category – 02	

13. ABSTRACT (Maximum 200 words)

Airloads measured on a two-bladed helicopter rotor in flight during the Ames' Tip Aerodynamic and Acoustic Test are compared with calculations from a comprehensive helicopter analysis (CAMRAD/JA), and the pressures compared with calculations from a full-potential rotor code (FPR). The flight-test results cover an advance ratio range of 0.19 to 0.38. The lowest-speed case is characterized by the presence of significant blade-vortex interactions. Good correlation of peak-to-peak vortex-induced loads and the corresponding pressures is obtained. Results of the correlation for this two-bladed rotor are substantially similar to those for three- and four-bladed rotors, including the tip-vortex core size for best correlation, calculation of the peak-to-peak loads on the retreating side, and calculation of vortex-induced loads on inboard radial stations. The higher-speed cases are characterized by the presence of transonic flow on the outboard sections of the blade. Comparison of calculated and measured airloads on the advancing side is not considered appropriate because the presence of shocks makes chordwise integration of the measured data difficult. However, good correlation of the corresponding pressures is obtained.

14. SUBJECT TERMS	15. NUMBER OF PAGES
Airloads correlations, Two-bladed rotor, Vortex-induced loads	27
	16. PRICE CODE A03

17. SECURITY CLASSIFICATION OF REPORT	18. SECURITY CLASSIFICATION OF THIS PAGE	19. SECURITY CLASSIFICATION OF ABSTRACT	20. LIMITATION OF ABSTRACT
Unclassified	Unclassified		

NSN 7540-01-280-5500